

Dispersion measurements with white-light interferometry

Scott Diddams and Jean-Claude Diels

Department of Physics and Astronomy, University of New Mexico, Albuquerque, New Mexico 87131

Received September 27, 1995; revised manuscript received January 2, 1996

White-light interferograms provide a simple, accurate, and physically intuitive picture of what happens to broadband optical pulses on transmission through, or reflection from, common optical materials. Quantitative measurement of group delay are made with an accuracy of ± 0.1 fs and with high spectral resolution. This measurement accuracy is applied to the determination of $d^2n/d\lambda^2$ and $d^3n/d\lambda^3$ of fused silica with an accuracy of $\pm 5 \times 10^{-5} \mu\text{m}^{-2}$ and $\pm 1 \times 10^{-3} \mu\text{m}^{-3}$, respectively. Further applications are found in the measurement of the dispersion of broadband mirrors and a multiple-quantum-well structure. © 1996 Optical Society of America

1. INTRODUCTION

White light, also known as thermal or Gaussian light, is often categorized as incoherent light and is therefore presumed to be of little use in a modern optics lab where lasers abound. Indeed, if one is to define temporal coherence as the ability of an electric field to interfere with a delayed version of itself, then the light from a helium–neon laser is certainly more coherent than that coming from a light bulb. However, white light does still remain coherent over a temporal delay of the order of femtoseconds, with the shortness being due to ultrafast Gaussian statistical temporal fluctuations. Only recently have laser systems also been able to generate optical pulses with a similarly short coherence lengths.^{1,2} The light coming from such a laser obeys different statistics (Poisson), and the spatial beam quality is typically much better than that from a white-light source; however, if one considers only linear correlations with slow detection, as are presented in what follows, it is impossible to distinguish between the two different kinds of light. In fact, for the measurements presented in this paper the light from a household bulb will give the same information as a pulse from a femtosecond laser system. Because of this, a white-light source, used in combination with a standard Michelson interferometer, has received increasing attention as a valuable tool in the study of the dispersive properties of optical materials. In particular, the measurement of group-delay dispersion, as well as of higher-order dispersion, introduced by the optical elements (mirrors, prisms, gain medium) in a femtosecond laser is of particular interest because the dispersion must be accurately controlled to yield the shortest pulses. It is the dispersion of the optical elements inside the laser cavity that tends to broaden the pulse temporally,^{3–5} unless a phase-modulation mechanism of sign opposite the dispersion exists in the cavity.^{6,7}

Initial dispersion measurements with white light involved measuring the centroid of the interference pattern produced with a Michelson interferometer and a filtered white-light source at various wavelengths.^{8–10} The relative group delay between the different frequency components introduced by an optical component placed in

one arm of the interferometer is obtained directly. The same information can be obtained by a Fourier transform of a single measurement when the full bandwidth of the white-light source is used.^{11,12} More recently, a two-dimensional, single-shot technique was introduced.¹³ The price to pay for the single-shot convenience is an increased demand on the flatness of the optics used, because the measurement cannot be made locally but requires a sample size of the same order as the detector size. This is what limits the relative error of the two-dimensional measurement to 10%. A broadband source, such as the fluorescence from a dye or a Ti:sapphire crystal pumped by an argon laser, is equally suitable, as was shown by Beck and Walmsley¹⁴ and Beck *et al.*,¹⁵ who made measurements of the group delay of various optical elements by using phase-locked interferometry. In this case high temporal and spectral resolution (0.1 fs and 0.1 nm, respectively) were obtained, but simplicity and affordability were sacrificed.

In what follows, we extend the technique introduced by Naganuma *et al.*,¹¹ improving the temporal accuracy to 0.1 fs and showing how it is possible to make absolute measurements of group delay. Because the technique used involves the Fourier transform of the measured interferogram, we can make the spectral resolution arbitrarily high by simply increasing the data collection in the time domain. The concepts associated with dispersion arise naturally and are well illustrated by the results and the theoretical description. Throughout all this, the analogy between white light and a femtosecond laser pulse is emphasized and the relevance of the measurements to the rapidly growing field of ultrafast lasers is discussed. These measurements not only have significance for those working with subpicosecond laser pulses but are also valuable for the accurate determination of the high-order derivatives of the index of refraction with respect to wavelength, as is shown below. In addition, we show how this technique can be applied to the characterization of multiple-quantum-well (MQW) samples. The growth of MQW structures involves a certain amount of uncertainty and one typically monitors and adjusts the growth process by measuring the reflection spectrum of the sample. The phase shift on reflection (or transmis-

sion), as obtained from a white-light interferogram, can be an extra piece of information in this evaluation process.

2. BALANCED AND UNBALANCED MICHELSON INTERFEROMETERS

To begin, let us consider the balanced Michelson interferometer shown in Fig. 1(a). By balanced, we mean that the path lengths in both arms of the interferometer are equal for all frequencies. The interferometer consists of a beam splitter and a compensator of the same material and equal thickness and of identical broadband nondispersive mirrors. The input field $\tilde{E}(t)$ is split by the beam splitter into the fields that travel through the two arms of the interferometer. If the mirror in one of the arms is translated a distance $x/2$, then the field in that arm will be delayed with respect to the field in the other arm by $\tau = x/c$. The delayed field is designated $\tilde{E}_1(t - \tau)$, and the undelayed field is called $\tilde{E}_2(t)$. With continuous translation of the mirror, a square-law detector at the output of the interferometer will measure the interference pattern (interferogram) that results from the two fields moving in and out of phase with respect to each other. As a function of delay, the interferogram has the form

$$I(\tau) \propto \langle \tilde{E}_1^2(t - \tau) \rangle + \langle \tilde{E}_2^2(t) \rangle + \langle \tilde{E}_1(t - \tau)\tilde{E}_2^*(t) \rangle \times \exp(-i\omega_l\tau) + \langle \tilde{E}_1^*(t - \tau)\tilde{E}_2(t) \rangle \exp(i\omega_l\tau), \quad (1)$$

where the angle brackets indicate the time averaging done by the detector. For this expression a complex representation of the fields has been used, such that $\tilde{E}_{1,2}(t) = \hat{E}_{1,2}(t)\exp(i\omega_l t)/2$, where $\hat{E}(t)$ is the complex amplitude function and ω_l is the average frequency of the radiation. For future reference we define the Fourier and the inverse Fourier transforms of this field to be

$$\begin{aligned} \tilde{E}(\omega) &= \int_{-\infty}^{+\infty} \tilde{E}(t)\exp(-i\omega t) dt, \\ \tilde{E}(t) &= \frac{1}{2\pi} \int_{-\infty}^{+\infty} \tilde{E}(\omega)\exp(i\omega t) d\omega, \end{aligned} \quad (2)$$

respectively. In many situations it is more convenient to work with a shifted frequency $\Omega = \omega - \omega_l$ and the complex envelope $\tilde{E}(t)$. It then follows from Eqs. (2) that

$$\begin{aligned} 2\tilde{E}(\Omega + \omega_l) &= \tilde{E}(\Omega) = \int_{-\infty}^{+\infty} \tilde{E}(t)\exp(-i\Omega t) dt, \\ \tilde{E}(t) &= \frac{1}{2\pi} \int_{-\infty}^{+\infty} \tilde{E}(\Omega)\exp(i\Omega t) d\Omega. \end{aligned} \quad (3)$$

We note that such a description is perfectly valid for all forms of light, regardless of the degree of coherence.

In relation (1) the first two terms are simply the constant average intensity, and the second two terms carry the interference information. These two interference terms have the form of first-order correlations, and in complete analogy to the definition of the complex electric field the correlation of the positive spectral components [those associated with the term containing $\exp(i\omega_l\tau)$] is defined as

$$\begin{aligned} \tilde{A}_1^+(\tau) &= \langle \tilde{E}_1^*(t - \tau)\tilde{E}_2(t) \rangle \exp(i\omega_l\tau) \\ &= \tilde{A}_1^+(\tau)\exp(i\omega_l\tau). \end{aligned} \quad (4)$$

The correlation involving the negative frequency components, $\exp(-i\omega_l\tau)$, can be neglected because it gives the same information as $\tilde{A}_1^+(\tau)$. Using the fact that the Fourier transform of a correlation of two functions is equal to the product of the Fourier transforms of the respective functions results in

$$\begin{aligned} \tilde{A}_1^+(\omega) &= \int_{-\infty}^{\infty} \tilde{A}_1^+(\tau)\exp(-i\omega\tau) d\tau \\ &= \tilde{E}_1^*(\omega)\tilde{E}_2(\omega) \end{aligned} \quad (5)$$

or, alternatively, in terms of the shifted frequency, in

$$\tilde{A}_1^+(\Omega) = \tilde{E}_1^*(\Omega)\tilde{E}_2(\Omega). \quad (6)$$

For the ideally balanced interferometer of Fig. 1(a) the fields in the two arms are identical, and $\tilde{E}_1(\Omega) = \tilde{E}_2(\Omega)$. The right-hand side of Eq. (6) is real and is simply the spectral intensity of the light $|\tilde{E}(\Omega)|^2$. This is just another way of saying that the correlation $\tilde{A}_1^+(\tau)$ is an autocorrelation, which is by definition an even function (symmetric about $\tau = 0$) and has a real Fourier transform. As Eq. (6) implies, when it is used in this way the Michelson interferometer is simply a Fourier spectrometer. We can make the conditions on this balanced Michelson interferometer more realistic by allowing for arbitrary amplitude and phase differences between the two fields. In this case Eq. (6) takes on the more general form

$$\begin{aligned} \tilde{A}_1^+(\Omega) &= \tilde{r}_{12}(\Omega)\tilde{E}_1^*(\Omega)\tilde{E}_2(\Omega) \\ &= \tilde{r}_{12}(\Omega)|\tilde{E}(\Omega)|^2, \end{aligned} \quad (7)$$

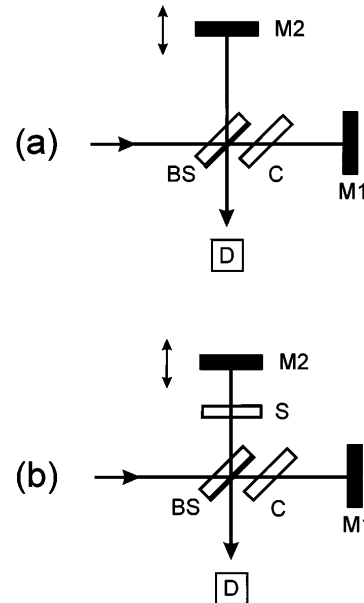


Fig. 1. (a) Balanced Michelson interferometer consisting of a beam splitter (BS), mirrors (M1, M2), and a compensator plate (C). (b) The unbalanced Michelson interferometer is identical to that in (a) with the exception of an extra piece of glass (S) in one arm. D's, detectors.

where $\tilde{r}_{12}(\Omega)$ is a complex, frequency-dependent function representing amplitude losses and any unbalanced phase shifts in the two arms of the interferometer.

It has just been shown how the Michelson interferometer can be used to give the spectrum of the source. Now we turn to the more interesting subject of how the properties of optical materials placed in one of the arms of the interferometer can be obtained. Consider the unbalanced Michelson interferometer of Fig. 1(b). With the insertion of a single piece of glass of thickness $d/2$, the field $\tilde{E}_2(t)$ will have traversed more glass than the field $\tilde{E}_1(t - \tau)$. The questions are: How will the fringe pattern be modified by having one beam traverse the additional length of glass, and which properties of the material can be inferred from these measurements? To answer these questions we begin by letting $\tilde{E}_1(\Omega)$ refer to the Fourier transform of the complex envelope $\tilde{E}_1(t - \tau)$, as given by Eqs. (3). In the frequency domain the field in the second arm is identical to that in the first arm, with the exception of the influence of the extra glass. We can account for this glass by using a complex optical transfer function $T(\Omega)\exp[-ik(\Omega)]$. This is simply a frequency-dependent amplitude filter and a path-length-dependent phase factor. The field in the second arm then takes on the form

$$\tilde{E}_2(\Omega) = T(\Omega)\tilde{E}_1(\Omega)\exp\left\{-id\left[k(\Omega) - \frac{\Omega + \omega_l}{c}\right]\right\}, \quad (8)$$

where the term $(\Omega + \omega_l)n_{\text{air}}d/c$ is the phase shift of the field in air ($n_{\text{air}} = 1$) and must be subtracted as shown. Below, we show that this term results only in a constant phase factor and a constant contribution to the group delay. Using this definition of $\tilde{E}_2(\Omega)$ in Eq. (7), we arrive at the following expression for the Fourier transform of the measured correlation with the unbalanced interferometer:

$$\begin{aligned} \tilde{\mathcal{A}}_2^+(\Omega) &= \tilde{r}_{12}(\Omega)|\tilde{E}(\Omega)|^2T(\Omega) \\ &\times \exp\left\{-id\left[k(\Omega) - \frac{\Omega + \omega_l}{c}\right]\right\}. \end{aligned} \quad (9)$$

It should be clear that when $\tilde{\mathcal{A}}_2^+(\Omega)$ of Eq. (9) is divided by $\tilde{\mathcal{A}}_1^+(\Omega)$ of Eq. (7) the terms $\tilde{r}_{12}(\Omega)$ and $|\tilde{E}(\Omega)|^2$ are eliminated, and one readily obtains the optical transfer function of the sample in both amplitude and phase. For transparent media $T(\Omega)$ can be considered a constant close to unity in the spectral region of interest. In this case the Fourier transform of the measured correlation for the unbalanced interferometer is identical to that of the balanced interferometer [Eq. (7)] with the addition of the phase term $\exp\{-id[k(\Omega) - (\Omega + \omega_l)/c]\}$.

It is this phase term that is of particular interest, because it describes the dispersive properties of the glass; we now consider it in further detail. We return to Eq. (8) and expand $k(\Omega)$ as a Taylor series about $\Omega = 0$ (i.e., the center frequency of radiation $\omega = \omega_l$); the field in the second arm then takes the form

$$\begin{aligned} \tilde{\mathcal{E}}_2(\Omega) &\approx T(\Omega)\tilde{\mathcal{E}}_1(\Omega) \\ &\times \exp\left\{-id\left[k_l + k_l'\Omega + \frac{k_l''}{2}\Omega^2 + \frac{k_l'''}{6}\Omega^3 + \dots\right]\right. \\ &\quad \left.+ i\frac{\Omega + \omega_l}{c}d\right\}, \\ \tilde{\mathcal{E}}_2(\Omega) &\approx T(\Omega)\tilde{\mathcal{E}}_1(\Omega) \\ &\times \exp\left\{-id\left[\frac{\omega_l}{c}(n_l - 1) + \left(k_l' - \frac{1}{c}\right)\Omega\right.\right. \\ &\quad \left.\left.+ \frac{k_l''}{2}\Omega^2 + \frac{k_l'''}{6}\Omega^3 + \dots\right]\right\}. \end{aligned} \quad (10)$$

In this expansion $k_l = 2\pi n_l/\lambda_l = \omega_l n_l/c$ is the magnitude of the wave vector at the wavelength ω_l for the glass of index n_l , and the higher-order terms are defined as follows:

$$\begin{aligned} k_l' &= \left(\frac{dk}{d\omega}\right)_l = \left[n_l + \omega_l\left(\frac{dn}{d\omega}\right)_l\right]\frac{1}{c} \\ &= \left[n_l - \lambda_l\left(\frac{dn}{d\lambda}\right)_l\right]\frac{1}{c} \end{aligned} \quad (11)$$

is the group delay per unit length of medium at the light frequency ω_l (or the inverse of the group velocity),

$$k_l'' = \left(\frac{d^2k}{d\omega^2}\right)_l = \frac{\lambda_l^3}{2\pi c^2}\left(\frac{d^2n}{d\lambda^2}\right)_l \quad (12)$$

describes the second-order dispersion (also called the group-delay dispersion per unit length) around the same frequency, and

$$k_l''' = \left(\frac{dk}{d\omega^3}\right)_l = -\frac{\lambda_l^4}{4\pi^2 c^3}\left[3\left(\frac{d^2n}{d\lambda^2}\right)_l + \lambda_l\left(\frac{d^3n}{d\lambda^3}\right)_l\right] \quad (13)$$

is the third-order dispersion per unit length. In the notation presented so far, the subscript l refers to the evaluation of the respective quantity at an arbitrarily chosen center wavelength (λ_l) or frequency (ω_l). We have chosen to refer to the derivatives of $k(\Omega)$ as the group delay and its higher-order dispersions, respectively, because such a convention follows most directly from the actual measurements as well as from the mathematical notation (i.e., k_l' has units of time/length, k_l'' has units of time²/length, etc.). It should be mentioned that the second-order term, $k'' = d/d\omega(1/v_g)$, is also commonly referred to as the group-velocity dispersion parameter. This is sometimes a source of confusion because the strictest definition of group-velocity dispersion is $dv_g/d\omega$. Another common definition of group-velocity dispersion is the derivative of v_g with respect to λ and can be expressed in terms of k'' as

$$\frac{dv_g}{d\lambda} = \frac{\omega^2 v_g^2}{2\pi c} \frac{d^2k}{d\omega^2}. \quad (14)$$

If a polynomial is numerically fitted to the phase of

relations (10) as obtained from the Fourier transform of the correlation, then the values of k_l , k_l' , k_l'' , and k_l''' can be related to the coefficients of the fit. As is explained below, experimental limitations generally prevent us from obtaining the zeroth- and the first-order terms of the expansion in relations (10). For applications involving ultrashort pulses this is of little consequence because the neglected zeroth- and first-order terms do not contribute to pulse shaping.

Each of the different terms of the expansion of $k(\Omega)$ in relations (10) plays a specific role in the actual form of a measured interferogram. As one might expect, the extra glass in one arm of the interferometer results in a longer path length and a corresponding shift in the time delay origin. It is known that an exponential factor linear in Ω transforms into a time shift. Therefore we find the correct expression for this delay by starting with the expansion in relations (10) limited to first order in $\Omega = \omega - \omega_l$:

$$\tilde{E}_2(\Omega) \approx \tilde{E}_1(\Omega) \exp\left(\frac{i\omega_l d}{c}\right) \times \exp\left[-id\left[k_l + \left(k_l' - \frac{1}{c}\right)\Omega\right]\right]. \quad (15)$$

The inverse Fourier transform of this expression, as given by Eqs. (3), then yields

$$\tilde{E}_2(t) = \exp[-i\omega_l d(n_l - 1)/c] \tilde{E}_1(t - \Delta t) \quad (16)$$

for the complex field envelope, where Δt is given by

$$\Delta t = d\left(k_l' - \frac{1}{c}\right) = \frac{d}{c} \left[(n_l - 1) - \lambda_l \left(\frac{dn}{d\lambda} \right)_l \right] = \frac{d}{v_g}. \quad (17)$$

In Eq. (17) we used the group velocity defined as $v_g = c/n_g = c/[n_l - \lambda_l(dn/d\lambda)_l]$. Apart from the phase factor in Eq. (16), we note that, as expected, the glass delays the envelope of the field passing through it. However, the delay is not simply the result of the difference of the phase velocity in air and glass given by $(n_l - 1)d/c$ but includes the term $-\lambda_l(dn/d\lambda)_l$. The interesting result is that a short pulse of radiation from a laser and the limited coherent structure of white light both propagate through a medium at the group velocity as defined above.

With a dispersive medium, a broadband source, or both, the second- and the higher-order terms of relations (10) are significant. The term k_l'' is the group-delay dispersion, and as its name implies it results in the temporal spreading of the various frequency subgroups that make up the light. In a normally dispersive medium this means that the red components travel ahead of the blue components. Similarly, the third-order dispersion k_l''' results in a further temporal separation of the frequency components. As will be shown, the second- and third-order terms are responsible for the stretching of a measured interferogram.

We note that relations (10) and the above discussion are not limited to transparent dielectric samples. We

can analyze the dispersive properties of a reflecting surface in the same way. However, in this situation the physical thickness is not usually a meaningful quantity, so the phase $k(\Omega)d$ of relations (10) is written simply as $\phi(\Omega)$. The group delay and its dispersions are then defined as $d\phi/d\Omega$, $d^2\phi/d\Omega^2$, and $d^3\phi/d\Omega^3$. In this situation the amplitude factor $T(\Omega)$ is the amplitude reflection spectrum and can no longer be considered constant. Equation (9) now contains the product of the spectrum of the source and the reflection spectrum of the sample.

3. MEASUREMENTS

A. Instrumentation

The actual recording of a white-light interferogram is quite simple, provided that the white-light fringes can be found in the first place. The fringes are readily observed only over a narrow range ($\pm 2 \mu\text{m}$ or $\pm 7 \text{fs}$) about the zero delay ($\tau = 0$), which is defined as the point for which the path lengths in both arms of the balanced interferometer are exactly equal. The experimental setup used for the following measurements is shown in Fig. 2. The small Michelson interferometer (a discontinued model from Gaertner Scientific) is constructed from a single cast block, making it very stable. In addition, a large reduction in the gearing enables one to scan through visible fringes with subwavelength accuracy. For all measurements the position of the movable mirror in the interferometer is translated with a slow dc motor ($\sim 60 \mu\text{m}$ -delay/min). However, the gearing and the driving motor suffer from variations in scan rate, so it is necessary continuously to monitor the interference fringes from a helium-neon laser sent through the same system. Measuring these fringes to a fraction of a wavelength enables one to determine the delay introduced by the translation of the mirror to within $\sigma_\tau = \pm 0.1 \text{fs}$ (or $\pm 30 \text{nm}$). The white-light source is an easily obtained halogen lamp (Osram 6 V, 20 W) and is placed at the focal length of a large-aperture lens to produce a nearly

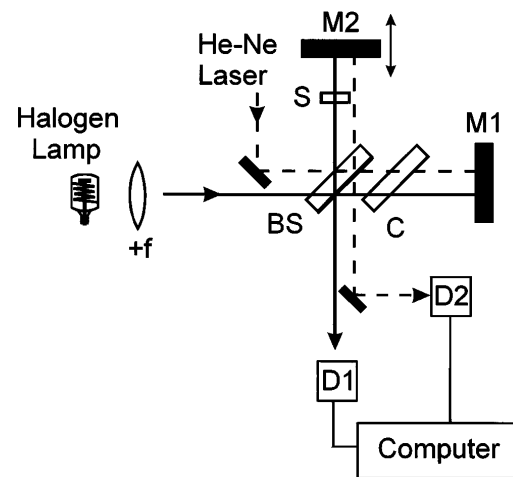


Fig. 2. Experimental setup for recording white-light interferograms. White light and helium-neon laser fringes are measured simultaneously with detectors D1 and D2 and stored in a computer. We use the helium-neon fringes to determine by what distance mirror M2 is moved. Other abbreviations as in Fig. 1.

collimated beam. Great care was taken in the selection of optics to ensure that the light in both arms experienced identical phase shifts over a broad bandwidth. The beam splitter and the compensator plate (Optics for Research) were polished side by side upon a large optically flat plate to yield the same thickness (3 mm) with a tolerance of a fraction of a wavelength. The partially reflective coating on the beam splitter was ~ 10 nm of Inconel. Although the metallic coating has higher absorptive losses, its bandwidth is greater than that of a dielectric. Similarly, the reflectors of the interferometer were metallic (Newport AL2). For all measurements the white light is detected with an avalanche photodiode (Hamamatsu S2381), and the calibrating helium–neon fringe pattern is simultaneously measured with a standard photodiode (Motorola MRD-510). The outputs of the diodes are sampled with an analog-to-digital card (Metrabyte DAS-16) mounted in a personal computer. For some measurements with the unbalanced interferometer, the white-light fringe contrast is poor, requiring the use of a mechanical chopper and a lock-in amplifier. Processing of the sampled data involves first calibrating the delay by use of the known period of the fringes of the helium–neon laser and then numerically computing the complex Fourier transform. A fast-Fourier-transform algorithm is not used because the delay points are not evenly spaced. Nonetheless, sampling of the data and computation time with a 486 processor takes only a few minutes. The spacing and the number of frequency points for which the transform is calculated are inputs to the algorithm; however, as with any Fourier spectrometer, the spectral resolution is ultimately given by the inverse of the total delay over which data are recorded. For example, a recording involving 300 fs of delay would have a spectral resolution of 5 nm near 750 nm. To obtain a resolution of 0.1 nm, one simply needs to extend the time delay range to approximately 15 ps.

B. Balanced Interferometer

A typical recording made with the balanced interferometer is shown in Fig. 3(a). The best least-squares fit of the data is obtained with the function

$$f(x) = g(x)h(x), \quad (18)$$

where $h(x)$ is a cosine with a Gaussian frequency variation of the form

$$h(x) = \cos\{[A \exp(-x^2/B) + C]x + D\} \quad (19)$$

and $g(x)$ is a Lorentzian envelope function of the form

$$g(x) = \frac{E}{1 + x^2/F} + G. \quad (20)$$

In Eqs. (18)–(20), $x = c\tau$ (x has units of micrometers) and the values of the fitting parameters are $A = 1.596$, $B = 2.428$, $C = 6.612$, $D = 5.468 \approx 7\pi/4 = -\pi/4$, $E = 1.062$, $F = 0.6295$, and $G = -0.04455$. The axis of symmetry of the Lorentzian envelope accurately defines the zero delay, and the oscillating fringe pattern is shifted in phase by $-\pi/4$ with respect to the zero-delay

point. This is the result of unequal phase shifts on reflection at the metallic beam splitter for the light approaching from the glass side as opposed to light approaching from the air side of the interface. We confirmed this by calculating the complex reflection coefficients of the air–metal–glass interface from both sides, using a standard matrix approach.¹⁶

The results of the subsequent Fourier transform of the data of Fig. 3(a) are presented in Fig. 3(b). In agreement with Eq. (7), the amplitude of the Fourier transform (curve i) yields the spectrum of the source. The limited spectral response of the silicon photodiode used in these measurements results in the sharp cutoff point in the measured spectrum at lower frequencies ($1.1 \mu\text{m}$ is the band-gap wavelength of silicon). This limitation in bandwidth may also explain in part the Lorentzian envelope of the interferogram of Fig. 3(a), which is not the expected envelope when one considers the statistical nature of white light. Further studies with wider band-

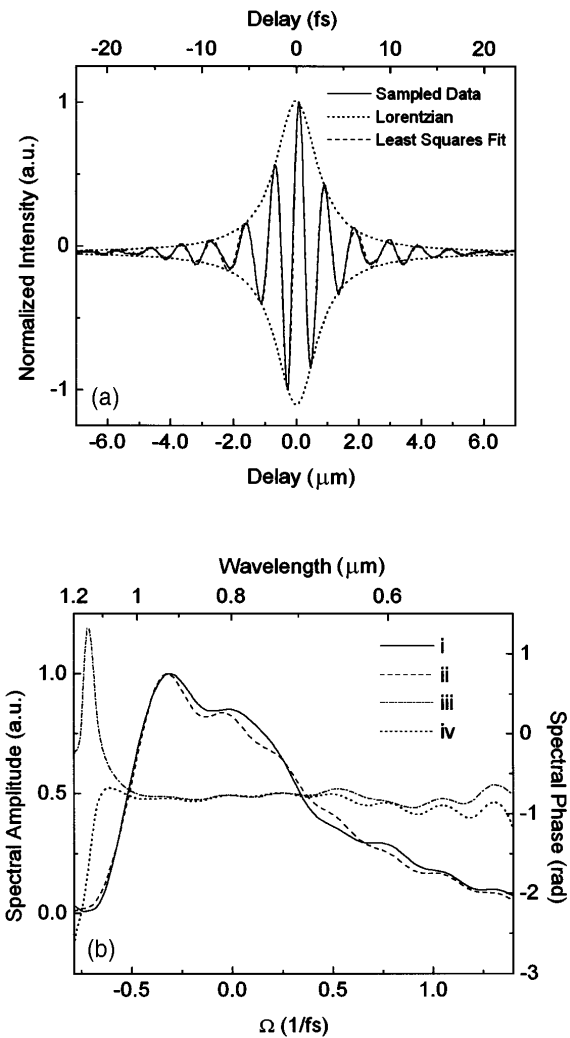


Fig. 3. (a) Interferogram with a balanced interferometer. A numerical fit of the sampled data and a Lorentzian envelope are also plotted. (b) Curves (i) and (iii) are the amplitude and the phase, respectively, of the Fourier transform of the actual data, and curves (ii) and (iv) are the amplitude and the phase of the Fourier transform of the functional fit to the data.

width detection are required for resolution of this issue. It is also interesting to note that the spectral amplitude in this case is not given by a double-sided exponential, as would be expected from a Lorentzian temporal envelope. This can be explained by the nonlinear chirp on the interferogram. The phase of the Fourier transform (curve iii) is also shown and is approximately constant, with its value close to $-\pi/4$, in agreement with the fitting of Eq. (19). The variation of the phase is only ± 0.1 rad in the range $-0.5 \leq \Omega \leq 0.5$. In the same range, the first derivative of the phase, which is the group delay, was found to vary by only ± 1 fs. This is the result of the instrument error, as represented by the phase of $\tilde{r}_{12}(\Omega)$ in Eq. (7). Because this error is now known, one can easily eliminate it in all subsequent measurements by simply subtracting it. Finally, the amplitude (curve ii) and the phase (curve iv) of the Fourier transform of the functional fit to the measured data are shown for comparison.

C. Measurement of k_l' and k_l'' for a Thin Sample

The interferogram recorded with a microscope cover slide, $d = 442 \pm 5 \mu\text{m}$, placed in one arm of the interferometer is shown in Fig. 4(a). In contrast to the balanced interferometer, the unbalanced interferometer results in an interferogram shifted with respect to the zero delay of the balanced interferometer. This shift is understood by the analogous description of an ultrashort coherent pulse, with an autocorrelation given by Eq. (18), propagating through the cover slide at the group velocity. The broadening of the interferogram, which leads to its asymmetry, is the result of the group-delay dispersion. As can be seen, the longer wavelengths arrive first and make for wider-spaced fringes. The light toward the blue end of the spectrum arrives later and comprises the more closely spaced fringes at the tail of the pattern.

It is not a trivial measurement to obtain the interferogram of Fig. 4(a) with the delay accurately referenced to the zero delay ($\tau = 0$) of the balanced interferometer. To accomplish this, we record the interferogram with the balanced interferometer, and then without stopping the translation of the mirror we insert the thin glass sample into one arm of the interferometer. Care must be taken to increase only the path length for the white light and not the helium-neon beam; otherwise the calibrated motion of the mirror will be lost. When the mirror arrives at the appropriate delay, as given by Eq. (17), the fringe pattern of Fig. 4(a) is recorded.

The amplitude and the phase of the Fourier transform of the interferogram in Fig. 4(a) are shown in Fig. 4(b) as a function of the shifted frequency $\Omega = \omega - \omega_l$, where $\omega_l = 0.375(2\pi) \text{ fs}^{-1}$ ($\lambda_l = 0.8 \mu\text{m}$). Here and in the following examples, the spectral phase is plotted only over the central region of the spectrum where the spectral amplitude is significant. In accordance with Eq. (9), the spectral amplitude is qualitatively unchanged from that presented in Fig. 3(b). The additional noise is the result of the larger amount of sampled data and the amplitude noise on those data. As shown by relations (10), when a polynomial of the form $\Phi = a_0 + a_1\Omega + a_2\Omega^2$ is fitted to the phase data in Fig. 4(b) the optical constants k_l' and k_l'' can be obtained directly. The term given by $a_0 = -\omega_l(n_l - 1)d/c$ cannot be retrieved because in the numerical computation of the Fourier transform the zero

point of the phase is arbitrarily chosen. Determination of this constant would require *a priori* knowledge of the index of refraction n_l . We note, however, that white-light interferometric techniques do exist for the accurate determination of the index of refraction.¹⁷ When those techniques are combined with the technique presented here, one could completely determine the index of a transparent medium and its higher-order derivatives to a high degree of accuracy.

From the actual polynomial fit to the phase data we obtain $a_1 = -d(k_l' - 1/c) = -772.5 \pm 0.1 \text{ fs}$, which gives $k_l' = 5.08 \pm 0.02 \text{ fs}/\mu\text{m}$. The error in a_1 comes directly from the uncertainty in the measured delay (σ_τ), whereas the accuracy of the value of k_l' could be improved by several orders of magnitude with a more accurate value for d . If the value of the index were known, one could use this value of k_l' to calculate the more commonly used value of $dn/d\lambda_l$ by using Eq. (11). We note that a_1 is simply the negative of the group delay given in Eq. (16). Comparison of this value with the actual delay of the interferogram of Fig. 4(a) shows good agreement. In fact, a direct measurement of the period T of the fringe about

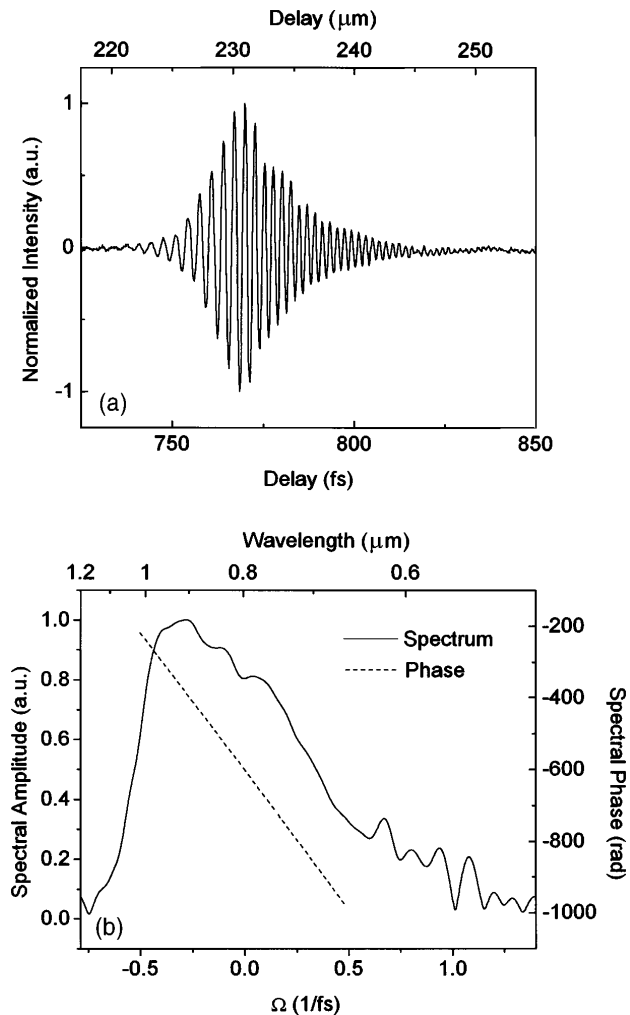


Fig. 4. (a) Interferogram with a microscope cover slide in one arm of the interferometer. (b) The result of the Fourier transform of these data in amplitude and phase. When a polynomial is fitted to the phase data, constants k_l' and k_l'' can be determined. The fit is not shown because it is indistinguishable from the data.

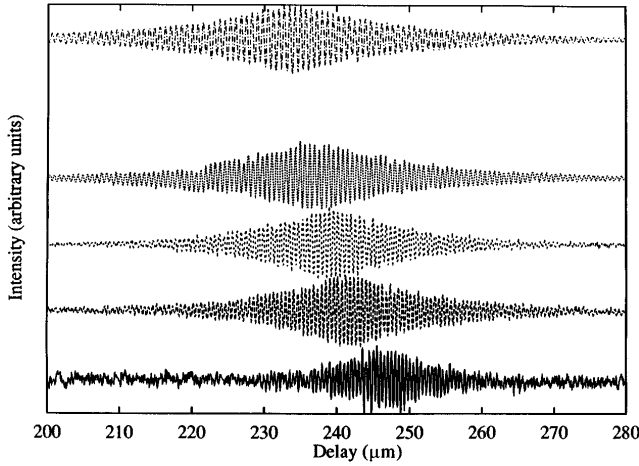


Fig. 5. Spectrally filtered interferograms recorded with a microscope cover slide in one arm of the interferometer. The white light is filtered before detection. The peak of the envelope for each interferogram is determined by the group delay at the center wavelength of each filter. From top to bottom, the center wavelengths of the filters are 750, 650, 600, 550, and 500 nm.

the delay of 772 fs yields a value of $T = 2.7$ fs, which is equal to $2\pi/\omega_l$.

In a similar fashion we can obtain the value of k_l'' and the related quantity $d^2n/d\lambda_l^2$. As shown in relations (10), $k_l''d/2$ is the coefficient of the quadratic term of the expansion of the phase. Using the same polynomial fit of the phase data as above, we get $a_2 = -k_l''d/2$, where a_2 is the fitting parameter. From Eq. (12) we can solve for $d^2n/d\lambda_l^2$ to obtain

$$\frac{d^2n}{d\lambda^2} = -a_2 \frac{4\pi c^2}{\lambda_l^2 d}. \quad (21)$$

The actual fit to the phase data yields $a_2 = -12.92 \pm 0.03$ fs². Inasmuch as $k_l''d/2$ is responsible for the stretching of the interferogram, we have estimated the relative error in a_2 as the ratio of the uncertainty in the delay to the spreading of the interferogram, which is $\sim 0.1/50 = 2 \times 10^{-3}$. This is also of the same order as the accuracy of the fit. We now arrive at the values of $k_l'' = 0.058 \pm 0.001$ fs²/μm, and $d^2n/d\lambda_l^2 = 0.064 \pm 0.001$ μm⁻². Because the material from which the lens cover slide is made is unknown, there are no data with which to compare these results. However, common optical glasses have similar values.

We further elucidate the concepts of group delay and group-delay dispersion by repeating the measurement shown in Fig. 4(a) but with various narrow-band optical filters placed in front of the source. By using a narrow-band filter ($\Delta\lambda \sim 5$ nm) we can neglect higher-order dispersion and observe only the delay introduced to the subgroup of frequencies transmitted by the filter. Interferograms that use five different filters are shown in Fig. 5. Because of the reduction in intensity we used a photomultiplier tube and a lock-in amplifier to take these data. These measurements are similar to those performed by Knox *et al.*, although in their study only relative delays were measured.⁸ As this figure shows, the peaks of the correlations for the different frequency groups are at different delays, with the correlation of the red light coming before the correlation of the blue light.

When these five correlations are compared with the single correlation shown in Fig. 4(a) we note that the delay positions for each frequency component are the same in both figures. Indeed, the single correlation of Fig. 4(a) contains all the same information available from an infinite number of correlations performed with a narrow-band or filtered source.

D. Measurement of k_l'' and k_l''' for a Thick Sample

Numerical and experimental convenience usually require that we ignore the first two terms in the expansion of relations (10). As we pointed out in Subsection 3.C, not only must the zero delay point of the balanced interferometer be determined with submicrometer accuracy but the delay from this point out to the measured interferogram must be measured with similar accuracy. This involves the sampling and storage of large amounts of data. For example, if d is only 1 mm and the data are sampled at a rate of 10 points/wavelength, approximately 17,000 points of noise-level signal have to be recorded for the determination of k_l' . Although we limit ourselves to the measurement of k_l'' and higher-order terms, it is more convenient to center the correlation $\hat{A}^+(\tau)$ approximately in the middle of the time domain (delay) to minimize the amplitude and the phase variation of the Fourier transform. We further note that, if measurements are made on a reflecting object rather than with a transparent dielectric, it becomes even more difficult to devise a measurement that allows one to obtain the zero-delay point of the balanced interferometer.

An illustrative example of the measurement of k_0'' and k_0''' is shown in Fig. 6, for which the sample was a piece of synthetic fused silica, $d = 3.957 \pm 0.005$ mm. As can be seen, the interferogram is now measured over a delay ten times greater than the data of Fig. 3(a), with the various frequency components spread out (from low to high) along the delay axis. Because of the difficulties described in the previous paragraph, the zero of the delay axis is arbitrary, although the relative accuracy is still of the order of ± 0.1 fs. The amplitude and the phase of the Fourier transform of these data are shown in Fig. 6(b). Once again, the spectrum is qualitatively the same as that obtained in Figs. 4(b) and 3(b), with the increased noise being due to amplitude fluctuations in the interferogram. For displaying the phase in Fig. 6(b), a polynomial ($\Phi = a_0 + a_1\Omega + a_2\Omega^2 + a_3\Omega^3$) was first fitted to the data, and then the constant and linear terms were subtracted, leaving only the dependence on the second- and the third-order dispersions. As can be seen, the agreement between the data and the third-order polynomial fit is excellent. From the fit we obtain $a_2 = -71.07 \pm 0.05$ fs² for the second-order coefficient, where the error is from the fit itself. This gives $k_l'' = 0.03592 \pm 0.00005$ fs²/μm and $d^2n/d\lambda_l^2 = 0.03962 \pm 0.00005$ μm⁻² at $\lambda_l = 800$ nm. In this measurement the third-order dispersion is also significant, yielding $a_3 = -18.1 \pm 0.2$ fs³ from the numerical fit of the phase data. This directly gives $k_l''' = 0.0274 \pm 0.0003$ fs³/μm. Using Eq. (13) and the calculated value of $d^2n/d\lambda_l^2$, we arrive at $d^3n/d\lambda_l^3 = -0.238 \pm 0.001$ μm⁻³. These values can be compared with $d^2n/d\lambda_l^2 = 0.0398$ μm⁻² and $d^3n/d\lambda_l^3 = -0.239$ μm⁻³, which were obtained from differentiation of an analytical expression for the index as

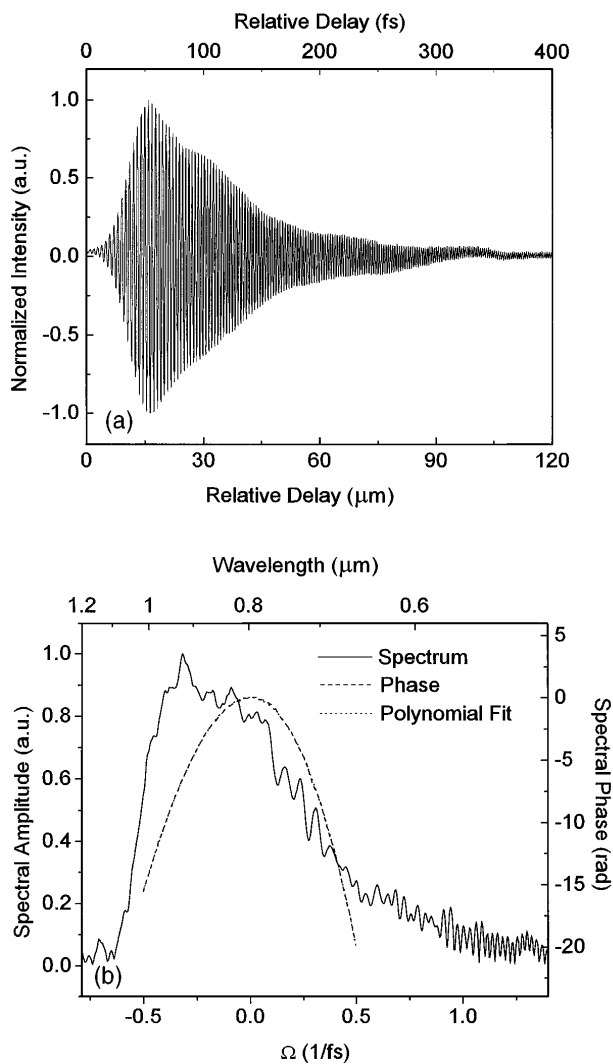


Fig. 6. (a) Interferogram with $d \approx 4$ mm of fused silica in one arm of the interferometer. (b) The result of the Fourier transform of these data. The constant and linear components of the spectral phase are subtracted, and the resulting curve is fitted with a third-order polynomial.

a function of wavelength.¹⁸ In both cases the measured results are more accurate than those calculated by differentiation because, even though the error in the index calculated from the analytical expression may be of the order of $\pm 10^{-5}$, the error in the higher derivatives is much greater.

E. Measurement of a Reflective Sample

As we mentioned above, this technique is not restricted to transparent dielectric samples. As an example, we studied a dielectrically coated high reflector made especially for use in a femtosecond Ti:sapphire laser (Newport UF.20) in the wavelength range of 0.7–0.9 μm . The resulting interferogram with one of the aluminum mirrors of the interferometer replaced by the Newport ultrafast mirror is shown in Fig. 7(a). It is interesting to note the modulation in the pattern following the main peak of the interferogram. It is unknown how the ~ 20 - μm (70-fs) period of the modulation of reflection relates to the actual construction of the reflector stack. The Fourier transform of these data yields the spectrum and the phase,

which are shown in Fig. 7(b). Curve i is the normalized reflection spectrum, where the measured spectrum of the white-light source [obtained from data similar to those of Fig. 3(a)] has been used for the normalization. As expected, the reflection spectrum is near unity over a broad bandwidth. Deviations from 1 are attributed to amplitude fluctuations in the white-light source and the sampled data. To obtain the correct reflection spectrum requires that the emission spectrum of the lamp be constant within 0.1% for both the reference interferogram and the interferogram of Fig. 7(a). The phase on reflection over the central part of the spectrum is shown by curve ii of the figure, where the phase constant and the term linear in Ω have been subtracted for display purposes. As detailed above, these terms do not contribute to the stretching of the interferogram or, for that matter, to the shaping of a femtosecond pulse. What remains of the phase still contains all the higher-order dispersion information. The solid curve iii is a fifth-order polynomial fit to the data. With an analytical form for the phase the second- and the third-order dispersions, $d^2\phi/d\Omega^2$ and

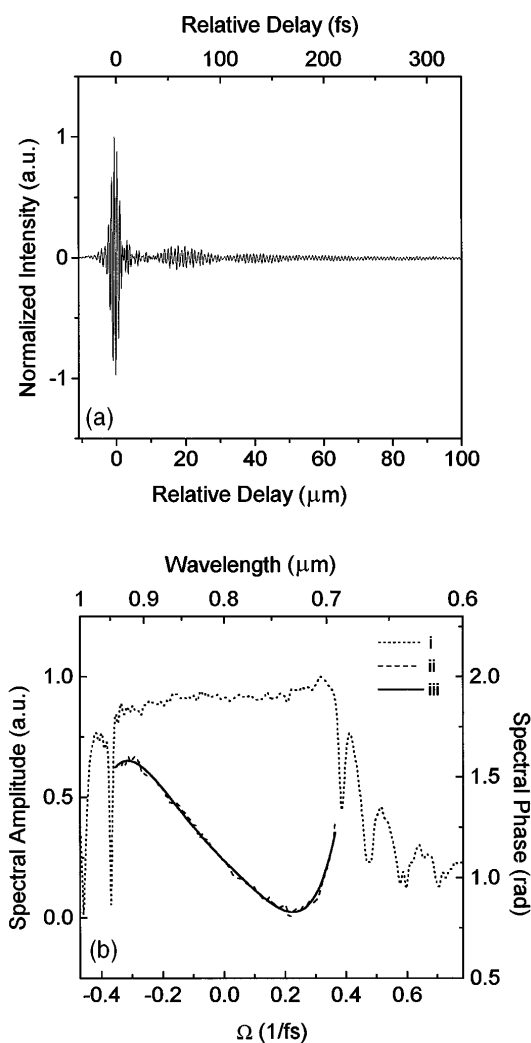


Fig. 7. (a) Interferogram for which one mirror of the interferometer was replaced by a mirror with a multilayer dielectric coating. (b) Curve (i) is the normalized amplitude of the Fourier transform (the reflection spectrum), curve (ii) is the phase of the Fourier transform with the constant and linear contributions subtracted, and curve (iii) is a fifth-order polynomial fit to the phase.

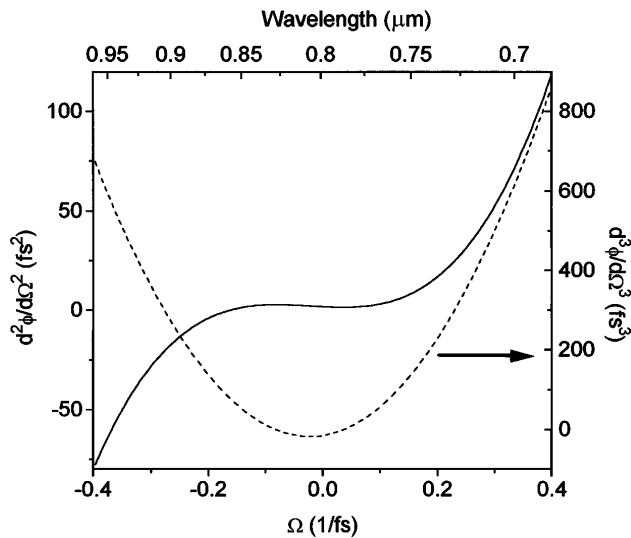


Fig. 8. Second and third derivatives of the spectral phase on reflection from a Newport UF.20 ultrafast mirror.

$d^3\phi/d\Omega^3$, can be calculated for all frequencies by differentiation of the polynomial. This was done, and the results are shown in Fig. 8. The estimated relative error in these curves is less than 4%. As is desired, both the second- and the third-order terms are close to zero in the center of the spectrum. There is also good agreement between these data and the theoretically calculated curves presented in the Newport catalog.¹⁹ We note that the technique demonstrated above can be used as a diagnostic tool not only for the development of ultrafast mirrors but also for the development of dispersion-compensating mirrors.^{13,20}

F. Measurement of a Multiple-Quantum-Well Sample

A major advantage of the white-light interferometer described here over a conventional spectrometer is that it provides both phase and amplitude information. This is an obvious advantage for reflective structures such as a Gires-Tournois interferometer, which has a constant amplitude reflection of unity and a large dispersion. It can also be valuable in the development of MQW structures, for which the reflection spectrum depends on numerous parameters such as composition, layer thickness, and interface properties. Typically, the parameters governing the growth process are adjusted such that only the measured reflection spectrum matches what is theoretically predicted. Unfortunately, more than one parameter can cause the same amplitude spectral shift. Therefore knowledge of the phase spectrum is an important additional piece of information in resolving these ambiguities. Measurements toward this end were carried out with a MQW structure designed to be a nonreciprocal gain source in a ring laser.²¹ Figure 9(a) shows an interferogram produced by the technique described above, in which one of the end mirrors of the Michelson interferometer has been replaced by the MQW sample. The Fourier transform of the data shown in Fig. 9(a) yields both the amplitude reflection spectrum [Fig. 9(b)] and the phase [Fig. 9(c)]. Because a constant phase shift and a term linear in Ω cannot be determined from the measurement, we have chosen to plot the first derivative of

the phase. In both Figs. 9(b) and 9(c) the experimental values are compared with those predicted by the theory. As can be seen, good agreement is found in some spectral regions, although further optimization in the growth process is required for a correct match. We note that the technique that we have described would be ideal for the characterization of other multilayer semiconductor devices such as the antiresonant Fabry-Perot saturable absorbers that were recently introduced for mode-locked solid-state lasers.²²

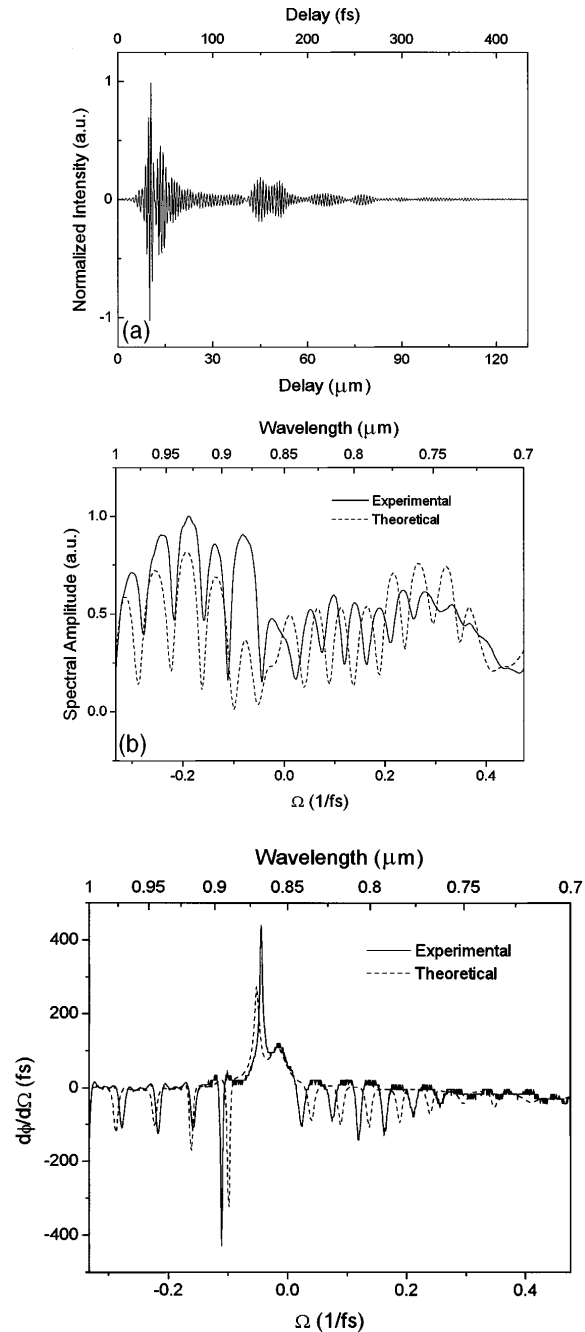


Fig. 9. (a) Interferogram for which one mirror of the interferometer is replaced by a MQW structure. (b) Theoretical and experimental reflection amplitudes for the MQW. The experimentally measured amplitude is not normalized by the spectrum of the source. (c) First derivative of the phase shift on reflection as obtained from both the theory and the experiment.

4. CONCLUSION

To account for the various characteristics observed in the measurements of Section 3 it is helpful to visualize white light as being made up of a superposition of the radiation from the many individual oscillators (atoms or molecules) that constitute the source. The temporal statistical fluctuations of this superposition are ultrafast, so white light behaves much as a femtosecond pulse. Indeed, the autocorrelation of Fig. 3(a) could be that of a laser pulse consisting of just a few optical cycles. It is for this reason that nonlinear correlations or broadband (fast) detection must be used to distinguish white light from a coherent femtosecond pulse. The analogy can be further extended to the data of Fig. 6(a). If we followed a femtosecond laser pulse through a piece of normally dispersive glass, it would become broadened and upchirped, with its red components preceding its blue components. The cross correlation of this chirped pulse with a delayed replica of the original pulse would also produce a result similar to that of Fig. 6(a). In fact, if the original pulse is short enough that it may be likened to a delta function, then the cross correlation simply yields the stretched pulse. From this point of view the interferogram of Fig. 6(a) is a good representation of what the stretched pulse would look like.

In summary, we have shown that a simple white-light interferometer can be a powerful tool for the accurate characterization of the dispersive properties of optical components. Specifically, we have measured the second- and the third-order dispersions of synthetic fused silica and a dielectrically coated high reflector near 800 nm. In the case of the fused silica the results are more accurate than values obtained by an analytical expression for the index of refraction, and in the case of the high reflector the results are in good agreement with calculated values. Finally, we presented an example of a metal organic chemical-vapor deposition-grown MQW structure to illustrate the usefulness of the technique in the diagnostic of complex multilayer structures. This technique and subsequent measurements should prove useful in the development of components for ultrashort pulse lasers, multilayer mirrors, and MQW structures.

ACKNOWLEDGMENTS

The authors thank Dushenka Myers-Taylor for the data of Fig. 3(a) and Paul Pulaski for the theoretical data of

Fig. 9. S. Diddams was supported in part as a graduate fellow of the Center for Advanced Studies of the University of New Mexico. This research was supported by the National Science Foundation under grant ECS-9219450 and by Continuum, Inc.

REFERENCES

1. R. L. Fork, C. H. Brito-Cruz, P. C. Becker, and C. V. Shank, *Opt. Lett.* **12**, 483 (1987).
2. J. Zhou, G. Taft, C.-P. Huang, M. M. Murnane, and H. C. Kapteyn, *Opt. Lett.* **19**, 1149 (1994).
3. M. T. Asaki, C.-P. Huang, D. Garvey, J. Zhou, H. C. Kapteyn, and M. M. Murnane, *Opt. Lett.* **18**, 977 (1993).
4. P. F. Curley, Ch. Spielmann, T. Brabec, F. Krausz, E. Wintner, and A. J. Schmidt, *Opt. Lett.* **18**, 54 (1993).
5. C. Spielmann, P. F. Curley, T. Brabec, and F. Krausz, *IEEE J. Quantum Electron.* **30**, 1100 (1994).
6. W. Dietel, J. J. Fontaine, and J.-C. Diels, *Opt. Lett.* **8**, 4 (1983).
7. J.-C. Diels and W. Rudolph, *Ultrashort Laser Pulse Phenomenon: Fundamentals, Techniques and Applications on a Femtosecond Time Scale* (Academic, Boston, Mass., 1995).
8. W. H. Knox, N. M. Pearson, K. D. Li, and C. A. Hirlimann, *Opt. Lett.* **13**, 574 (1988).
9. K. D. Li, W. H. Knox, and N. M. Pearson, *Opt. Lett.* **14**, 450 (1989).
10. Z. Bor, K. Osvay, B. Rácz, and G. Szabó, *Opt. Commun.* **78**, 109 (1990).
11. K. Naganuma, K. Mogi, and H. Yamada, *Opt. Lett.* **17**, 393 (1990).
12. K. Naganuma and H. Yasaka, *IEEE J. Quantum Electron.* **27**, 1280 (1991).
13. A. P. Kovács, K. Osvay, Z. Bor, and R. Szipöcs, *Opt. Lett.* **20**, 788 (1995).
14. M. Beck and I. A. Walmsley, *Opt. Lett.* **15**, 492 (1990).
15. M. Beck, I. A. Walmsley, and J. D. Kafka, *IEEE J. Quantum Electron.* **27**, 2074 (1991).
16. M. V. Klein and T. E. Furtak, *Optics* (Wiley, New York, 1986).
17. V. N. Kumar and D. N. Rao, *J. Opt. Soc. Am. B* **12**, 1559 (1995).
18. *Optics Guide 5* (Melles Griot, Irvine, Calif., 1990).
19. *Newport Catalog* (Newport Corporation, Irvine, Calif., 1994).
20. A. Stingl, C. Spielmann, F. Krausz, and R. Szipöcs, *Opt. Lett.* **19**, 204 (1994).
21. P. Pulaski and J.-C. Diels, in *Conference on Lasers and Electro-Optics*, Vol. 15 of OSA Technical Digest Series (Optical Society of America, Washington, D.C., 1995), p. 153.
22. L. R. Brovelli, U. Keller, and T. H. Chiu, *J. Opt. Soc. Am. B* **12**, 311 (1995).